Photothermal measurement of thermal anisotropy in pyrolytic graphite

J. Hartmann, P. Voigt, M. Reichling, E. Matthias

Freie Universität Berlin, Arnimallee 14, D-14195 Berlin, Germany
(Fax: + 49-30/838-6059, E-mail: REICHLING@matth1.physik.fu-berlin.de)

Abstract. We investigated the anisotropic thermal conductivity in pyrolytic graphite by thermoreflectance. A laser-heated circular spot on a surface perpendicular to the planes developed into an elliptical temperature distribution which was recorded by a raster scanning technique at modulation frequencies ranging from 600 Hz to 100 kHz. The ratio of in-plane and perpendicular thermal conductivity was determined by fitting the phase of the temperature data with an analytical model, and was found to decrease with increasing modulation frequency. Highest conductivity values were considerably smaller than previously published data based on steady-state measurements. The frequency dependence and additional features in the phase profiles at high frequencies are discussed in view of sample surface preparation and the local nature of the thermoreflectance measurement.

PACS: 66.70. + f

Heat transport in inhomogeneous or anisotropic media is of interest, e.g. in thin film technology and in electronic device design. Thermal characteristics of thin films strongly depend on the preparation procedure and may significantly differ from bulk values [1]. Often thin films exhibit a thermal anisotropy with different in-plane and perpendicular thermal conductivities. Shaw-Klein et al. [2] measured thermal anisotropies in rare-earth transition metal films, while Graebner et al. [3] reported about the large thermal anisotropy in chemical-vapor-deposited diamond films. Extensive studies have been carried out by various authors of the anisotropy in high-T_C superconducting materials [4–6] and liquid crystals [7–9]. McCurdy et al. [10] measured heat conduction in cubic single crystals in the boundary scattering regime and found an anisotropy depending on the orientation of the crystals with respect to the heat conduction direction. Gan and Zhang [11] reported about thermal anisotropy in quartz. Some authors also investigated the anisotropic thermal behavior of organic and composite materials, e.g.,

Quelin et al. [12] determined the thermal properties of an orthorhombic polydiacetylene sample, and Inglehart et al. [13] measured the thermal conductivity of a carbon-epoxy composite.

In the present paper, we demonstrate thermal anisotropy in a bulk graphite sample utilizing the thermoreflectance technique [14] as a local probe for the surface temperature variation induced by a modulated Ar^+-laser beam. The measurement scheme is similar to the one developed by Visser et al. [15], who observed the broadening of the modulated temperature profile on sample surfaces by an IR-video camera.

Focussing an intensity-modulated Gaussian laser beam on an absorbing surface yields a periodic primary heat source with circular symmetry. The time evolution of the resulting temperature profile depends on the thermal characteristics of the sample. In case of a sample with isotropic thermal properties, the profile maintains its spherical shape; in the anisotropic case, however, one obtains an ellipsoidal distribution with the greater axis in the direction of higher thermal conductivity.

For optically and thermally thick bulk samples, the dispersion relation of harmonic heat flow in the one-dimensional case is $q^2 = i\omega/D$, where q is the thermal wave number, ω the angular frequency of the harmonic heat source and $D = K/\rho c$ the thermal diffusivity, with K being the thermal conductivity and ρc the volume specific heat at constant pressure. The temperature along one direction obeys an $\exp(iqx - i\omega t)$ periodicity with heavy damping. After one thermal length $L_{th} = \sqrt{2D/\omega}$, the temperature drops to $1/e$ of the starting value. The phase lag between the periodic heat source and the temperature at a distance Δx from the source is $\Delta\theta = \sqrt{\omega/2D}\,\Delta x$. Using this relation, the determination of the thermal diffusivity is straightforward [16].

The problem of three-dimensional isotropic heat flow was solved for bulk and layered systems [17–19]. Here we need a solution of the anisotropic three-dimensional heat diffusion equation. Several authors dealt with this problem, for example, Lu [20] solved the stationary heat diffusion equation. In our experiment we used a modulated heat source and hence need a solution of the
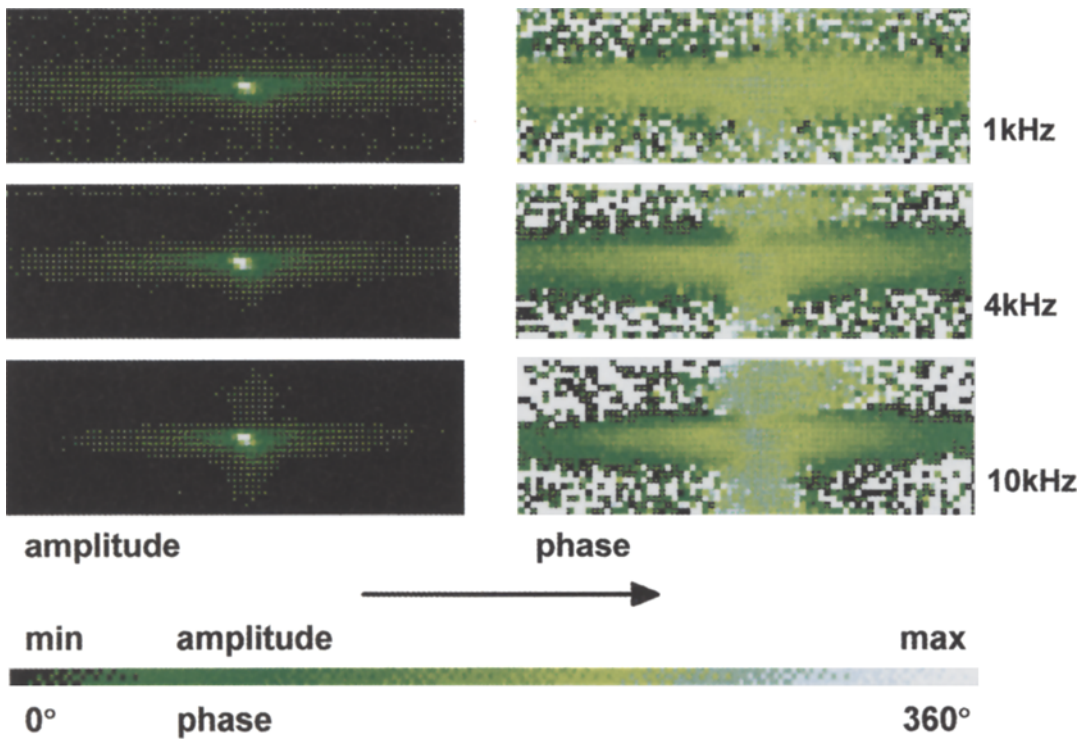
Fig. 1. Amplitude and phase images (0.9 mm × 0.3 mm) of the modulated temperature distribution on a pyrolytic graphite sample, cut perpendicular to the planes. The direction of the planes is indicated by the *arrow*

time-dependent heat diffusion equation. Only a few papers addressed this topic [12, 21, 22]. We take the solution given by Grönbeck and Reichling [22], who calculated the temperature distribution for an anisotropic bulk sample with consideration of the penetration depth of the laser light. In this theory, for certain parameter combinations convergence problems arise when evaluating the integrals involved. In those cases we used a simpler analytical solution for the case of surface absorption which is outlined in the appendix.

1 Experimental

Measurements were performed on pyrolytic graphite. This particular form of graphite has a layered structure resulting in a strong anisotropy between the thermal conductivity in-plane and perpendicular to it. In the literature values of 1960 W/mK for the in-plane value of the thermal conductivity and 5.7 W/mK for the perpendicular direction at room temperature are reported [23], which amounts to a ratio of 344.

To visualize the anisotropy, we cut the pyrolytic graphite perpendicular to the layers and polished the surface with diamond paste in successive steps with 15 to 0.3 μm grain size to obtain optical quality. However, inspection of the polished surface by an optical microscope showed, that incomplete polishing results in scratches of some 10 μm in height. Additionally, the sample surface was covered with a thin layer of gold to enhance the thermoreflectance signal. The gold layer was thermally evaporated and had a thickness below 50 nm.

The experimental setup is described in detail elsewhere [24]. In the experiments reported here, the relative position of probe and pump beam was raster-scanned to obtain an image of the surface temperature distribution. The Ar^+-laser beam was intensity modulated by an acousto-optical modulator, and modulation frequencies ranged from 600 Hz to 100 kHz. The temperature profile induced by the heating Ar^+-laser beam generates a modulated surface reflectivity change which was measured via reflectance of the HeNe probe beam. The intensity modulation of the reflected HeNe beam is proportional to the surface temperature ΔT via $\Delta R/R = \Delta T/R\, dR/dT$ with R being the surface reflectivity. The heated spot had a radius of 50 μm while the probe beam was focused to 20 μm diameter. Both, amplitude and phase of the induced surface temperature were recorded as a function of pump beam position while the probe beam was kept at a fixed position at the surface. We repeated few selected experiments in a photothermal microscope with tighter focused laser beams to study the influence of pump and probe beam size on the conductivity results. Beam diameters were varied by using microscope objectives of different magnification where a minimum spot size of 1.5 μm was obtained.

2 Results and discussion

Figure 1 shows amplitude and phase of the temperature distribution at frequencies 1, 4 and 10 kHz. At all modula-
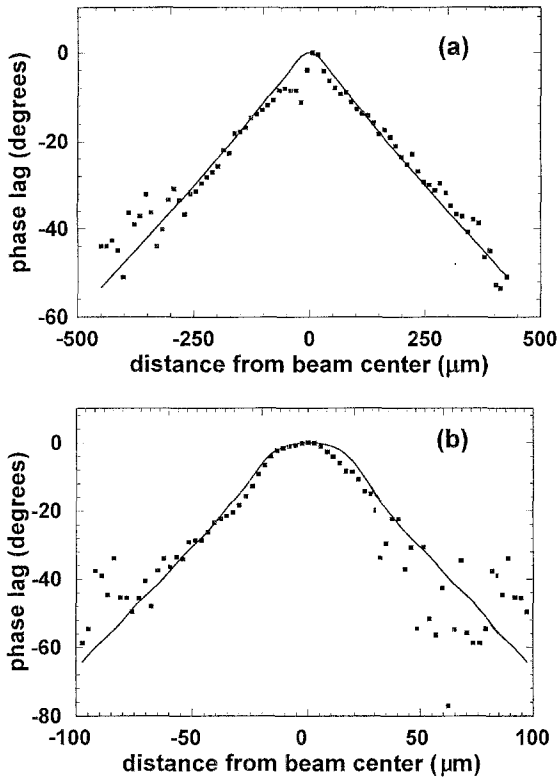
Fig. 2a, b. Phase of the thermal profiles extracted from the 2D-images of Fig. 1 at 1 kHz. **a** High conductivity direction, **b** low conductivity direction. *Solid lines* are fits to the experimental data yielding a thermal conductivity of 1300 W/mK in plane and 20 W/mK perpendicular to the planes
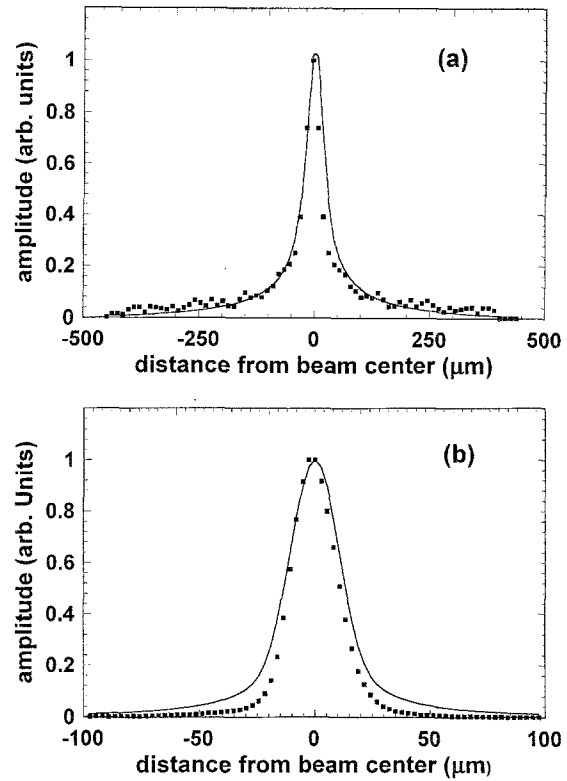

Fig. 3a, b. Amplitude profiles extracted from the 2D images of Fig. 1 at 1 kHz. **a** High conductivity direction, **b** low conductivity direction. The *solid lines* are calculated with the fit parameters to the phase profiles

tion frequencies, both amplitude and phase images exhibit elliptical temperature profiles characterizing the thermal anisotropy of the sample. The relation of the main axes of the ellipse yields a first qualitative value for the aniso-tropic thermal conductivity in the perpendicular directions.

For a quantitative analysis we take cuts through the two-dimensional temperature images and fit analytical solutions to the resulting amplitude and phase profiles. Figure 2 shows measured phase profiles and fitted curves for the in-plane and perpendicular direction at 1 kHz, while Fig. 3 illustrates the amplitude results. The fit of the phase profiles yields (1300 ± 200) W/mK for in-plane and (20 ± 7) W/mK for perpendicular thermal conductivity. As the amplitude is more sensitive to experimental distur-bances, we mostly analyzed the phase variation across the thermal profile. So the curves plotted in the amplitude pictures are no fits, but demonstrate the consistency of the parameter values obtained by the fits to the phase data. In both cases we get a good agreement with the experiment.

Results of measurements at various frequencies are shown in Fig. 4. The plot represents the ratio of the in-plane conductivity to the perpendicular conductivity. It can clearly be seen that the ratio decreases from a value of 60 down to 10 while the frequency increases from 600 Hz to 100 kHz. The large scatter in the data and error bars result from sample preparation as will be discussed below. Generally, all measured features were reproducible when measured at different locations on the sample surface,
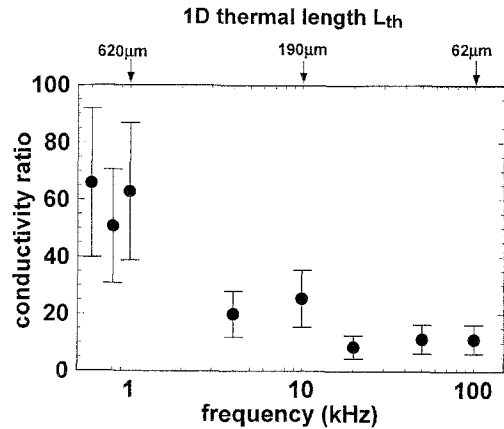

Fig. 4. Plot of the ratio of in-plane to perpendicular thermal con-ductivities as a function of the modulation frequency

however, due to the structural inhomogeneity of the sur-face on a scale comparable to the thermal diffusion length, quantitative results varied for different locations.

The maximum conductivity ratio obtained in Fig. 4 significantly differs from the literature values, as we measure a lower thermal conductivity in the in-plane direction and a higher conductivity in the out-of-plane one. According to the published steady-state data [23], a conductivity ratio of about 300 was expected. We as-cribe this strong discrepancy to two reasons, namely,

sample preparation and the local nature of our photothermal detection scheme.

Polishing the surface with the diamond grain powder produces disorder of the layered structure of the pyrolytic graphite and, therefore, alters thermal characteristics in the topmost layers and results in a more isotropic thermal behavior. Additionally, the gold coating reduces the anisotropy by enhancing surface thermal conductivity. To estimate the influence of the gold layer, the isotropic theory for layered samples [19] was applied. It yields that a gold layer of 50 nm enhances the thermal conductivity perpendicular to the layers by 20% in case of a 1 kHz measurement.

This interpretation is supported by the measurements at higher frequencies. There an additional feature in the center of the temperature profiles arises, most clearly seen in the phase profile obtained at 10 kHz in Fig. 1. The smear-out in the phase profiles is most likely due to the disordered material structure in the topmost layers, generated by surface polishing. Since only thermal properties within one thermal length L_{th} affect the surface temperature distribution [16], in the high-frequency regime the surface temperature distribution is more sensitive to both polishing effects and gold layer and, therefore, phase images of the surface temperature exhibit a more isotropic behavior. Measured values provide a 1D in-plane diffusion length of 60 µm for 100 kHz, however, the 3D in-plane thermal diffusion length is considerably smaller and compares to the expected depth of polishing scratches of some 10 µm resulting from the polishing procedure. On the other hand, we find a diffusion length of 600 µm at the lowest frequencies that is larger than the thickness of the disturbed surface layer. To confirm this interpretation, we performed comparative transient thermal grating measurements [25]. The penetration depth was at most 40 µm for this experiment and the measurements did not exhibit any thermal anisotropy.

The strongly reduced in-plane conductivity presumably also results from the small surface area heated by the Ar^+-laser and probed by the HeNe beam. While in a steady-state measurement involving a large thermally active volume the reduction of heat transfer in a disrupted surface layer is negligible, it is crucial for heating and probing with a highly focussed laser beam where local thermal resistances between surface grains may thermally alter the probed volume. This interpretation also explains the observation we made when varying the foci of the involved laser beams. We found that the measured in-plane conductivity was reduced even more when using a highly focussed heating and probe beam of less than 2 µm diameter, i.e., a further reduction of the heated and probed area enhances the influence of the local structure. The dimension of the sample available allows the use of maximum beam diameters in the 100 µm range and so it is not possible to find out whether a further increase of beam diameter yields a thermal conductivity ratio closer to the literature value. However, from the trend in the data in Fig. 4, we expect a saturation at the highest values we measured.

In summary, it can be concluded that a local photothermal measurement as presented here is well able to detect and qualitatively characterize thermal anisotropy;

however, quantitative data analysis may be strongly influenced by local effects due to the surface structure and coating and requires great care in adjusting experimental parameters, especially the laser focus and the modulation frequency.

Appendix

The three-dimensional heat conduction equation in the case of modulated Gaussian laser light absorbed in an infinitely thin surface layer as heat source can be written as:

$$K_1 \frac{\partial^2 T}{\partial x^2} + K_2 \frac{\partial^2 T}{\partial y^2} + K_3 \frac{\partial^2 T}{\partial z^2} - i\omega\rho c$$
$$= Q_0 \exp\left(-\frac{x^2 + y^2}{a^2}\right)\delta(z), \tag{1}$$

with the boundary condition at the rear side of the sample

$$K_3 \frac{\partial T}{\partial z} = 0, \tag{2}$$

where K_1, K_2 and K_3 are the thermal conductivities in x, y and z direction, respectively. Q_0 is the absorbed peak energy per unit area and a is the beam waist. The other parameters are given in the introduction. The general solution of (1) is [16]

$$A_n \cos\left(\frac{n\pi x}{L_1}\right) \cos\left(\frac{m\pi y}{L_2}\right) \cosh\left[(L_3 - z)\gamma\right], \tag{3}$$

where L_1, L_2 and L_3 are the sample dimension in x, y and z direction, respectively. The variable γ is defined as

$$\gamma^2 = \beta^2 + \frac{n^2\pi^2}{L_1^2}\frac{K_1}{K_3} + \frac{m^2\pi^2}{L_2^2}\frac{K_2}{K_3} \quad \text{with} \quad \beta = i\frac{\omega\rho c_p}{K_3}. \tag{4}$$

Consideration of the boundary condition yields the final solution to the anisotropic heat conduction equation in form of a Fourier series:

$$T(x, y, 0) = \frac{Q_0}{L_1 L_2 K_3} \sqrt{\frac{K_1 K_2}{K_3^2}} \sum_{n,m}^{\infty} \frac{\cosh(L_1\gamma)}{\sinh(L_2\gamma)} \cos\left(\frac{n\pi x}{L_1}\right)$$
$$\times \cos\left(\frac{n\pi y}{L_2}\right) \exp\left[-\frac{\pi^2 a^2}{4}\left(\frac{n^2}{L_1^2} + \frac{m^2}{L_2^2}\right)\right]. \tag{5}$$

References

1. J. Hartmann, O. Nilsson, J. Fricke: High Temp. High Press. 25, 403 (1993)
2. L.J. Shaw-Klein, T.K. Hatawar, S.J. Burns, S.D. Jacobs, J.C. Lambrocoulos: J. Mater. Res. 7, 329 (1992)
3. J.E. Graebner, S. Jin, J.A. Herb, C.F. Gardinier: J. Appl. Phys. 76, 1552 (1994)

4. J.T. Fanton, D.B. Mitzi, A. Kapitulnik, B.T. Khuri-Yakub, G.S. Kino: Appl. Phys. Lett. **55**, 598 (1989)
5. X.D. Wu, J.G. Fanton, G.S. Kino. S. Ryu, D.B. Mitzi, A. Kapitulnik: Physica C **218**, 417 (1993)
6. X.D. Wu, G.S. Kino, J.T. Fanton, A. Kapitulnik: Rev. Sci. Instrum. **64**, 3321 (1993)
7. M. Gharbia, A. Hadj-Sahraoui, G. Louis, A. Gharabi, P. Peretti: In *Photoacoustic and Photothermal Phenomena II*, ed. by J.C. Murphy, J.W. Maclachlan-Spicer, L. Aamodt, B.S.H. Royce, Springer Ser. Opt. Sci., Vol. 62 (Springer, Berlin, Heidelberg 1990)
8. C. Glorieux, E. Schoubs, J. Thoen: In *Photoacoustic and Photothermal Phenomena II*, ed. by J.C. Murphy, J.W. Maclachlan-Spicer, L. Amodt, B.S.H. Royce, Springer Ser. Opt. Sci., Vol. 62 (Springer, Berlin, Heidelberg 1990) p. 297
9. F. Enguehard, A. Déom, D. Balageas: In *Photoacoustic and Photothermal Phenomena III*, ed. by D. Bicanic Springer Ser. Opt. Sci., Vol. 69 (Springer, Berlin, Heidelberg 1992) p. 537
10. A.K. McCurdy, H.J. Maris, C. Elbaum: Phys. Rev. B **2**, 4077 (1970)
11. C. Gan, X. Zhang: In *Photoacoustic and Photothermal Phenomena*, ed. by P. Hess, J. Pelzel Springer Ser. Opt. Sci., Vol. 58 (Springer, Berlin, Heidelberg 1988) p. 335
12. X. Quelin, B. Perrin, G. Louis, P. Peretti: Phys. Rev. B **48**, 3677 (1993)
13. L.J. Inglehart, F. Lepoutre, F. Charbonnier: J. Appl. Phys. **59**, 234 (1986)
14. A. Rosencwaig, J. Opsal, W.L. Smith, D.L. Willenborg: Appl. Phys. Lett. **46**, 1013 (1985)
15. E.P. Visser, E.H. Versteegen, W.J.P. van Enckevort: J. Appl. Phys. **71**, 3238 (1992)
16. H.S. Carslaw, J.C. Jaeger: Conduction of Heat in Solids (Oxford Univ. Press, New York 1959)
17. W.B. Jackson, N.M. Amer, A.C. Boccara, D. Fournier: Appl. Opt. **20**, 1333 (1981)
18. J. Opsal, A. Rosencwaig, D.L. Willenborg: Appl. Opt. **22**, 3169 (1983)
19. M. Reichling, H. Grönbeck: J. Appl. Phys. **75**, 1914 (1994)
20. Y.-F. Lu: J. Appl. Phys. **72**, 4893 (1992)
21. M.V. Iravani, M. Nikoonahad: J. Appl. Phys. **62**, 4065 (1987)
22. H. Grönbeck, M. Reichling: J. Appl. Phys. **78**, 6408 (1995)
23. R.C. Weast (ed.) : *Handbook of Chemistry and Physics* (CRC, Cleaveland 1974)
24. M. Reichling, E. Welsch, A. Duparré, E. Matthias: Opt. Eng. **33**, 1334 (1994)
25. O.W. Käding, E. Matthias, R. Zachai, H.-J. Füßer, P. Münzinger: Diamond Rel. Mater. **2**, 1185 (1993)